

Journal of Materials Chemistry C

Accepted Manuscript



This is an *Accepted Manuscript*, which has been through the Royal Society of Chemistry peer review process and has been accepted for publication.

Accepted Manuscripts are published online shortly after acceptance, before technical editing, formatting and proof reading. Using this free service, authors can make their results available to the community, in citable form, before we publish the edited article. We will replace this *Accepted Manuscript* with the edited and formatted *Advance Article* as soon as it is available.

You can find more information about *Accepted Manuscripts* in the [Information for Authors](#).

Please note that technical editing may introduce minor changes to the text and/or graphics, which may alter content. The journal's standard [Terms & Conditions](#) and the [Ethical guidelines](#) still apply. In no event shall the Royal Society of Chemistry be held responsible for any errors or omissions in this *Accepted Manuscript* or any consequences arising from the use of any information it contains.

Structures and Charge Transport Properties of “Selenosulflower” and its Selenium Analogue “Selflower”: Computer-Aided Design of High-Performance Ambipolar Organic Semiconductors

Jun Yin, Chaitanya Kadali, Xue-Hai Ju*

Key Laboratory of Soft Chemistry and Functional Materials of MOE, School of Chemical Engineering, Nanjing University of Science and Technology, Nanjing 210094, P. R. China

Abstract: A novel crystal structure of octaseleno[8]circulene ($C_{16}Se_8$, we named it selflower) was predicted on the basis of sym-tetraselenatetrathio[8]circulene crystal ($C_{16}S_4Se_4$, selenosulflower). The charge transport properties of selenosulflower and its selenium analogue of selflower as potential ambipolar materials were investigated by the density functional theory (DFT) coupled with the incoherent charge-hopping model. Insights into their geometric and electronic structures, frontier molecular orbitals, reorganization energies and transfer integrals, anisotropic mobilities as well as band structures of the two novel materials were provided in detail. The gap of the frontier molecular orbitals decreases when all sulfur atoms of $C_{16}S_4Se_4$ are substituted by selenium, which improves the charge transfer efficiency. The predicated hole and electron mobilities of $C_{16}Se_8$ are 1.03 and 1.26 $cm^2 \cdot V^{-1} \cdot s^{-1}$, respectively. $C_{16}S_4Se_4$ has hole mobility of 0.49 $cm^2 \cdot V^{-1} \cdot s^{-1}$ and electron mobility of 0.74 $cm^2 \cdot V^{-1} \cdot s^{-1}$. Both circulenes exhibit electron-dominated ambipolar performance. The small reorganization energy and larger transfer integral originated from the face to face π - π stacking lead to large charge mobility for the novel compound $C_{16}Se_8$. In the viewpoint of transfer integral, the electron coupling among the dominant hopping pathways indicates that the

* Corresponding author. E-mail: xhju@njust.edu.cn; Tel: +86 25 84315947-801; fax: +86 25 84431622

charge transport processes take place in the parallel dimers with π - π interaction. The two materials exhibit remarkable angular dependence of mobilities and anisotropic behaviors. The newly designed “selflower” $C_{16}Se_8$ is a novel organic semiconductor and worthy to synthesize.

Keywords: Tetraselenatetrathio[8]circulene (selenosulflower), Octaseleno[8]circulene (selflower), Hole and electron mobilities, Density functional theory (DFT), p-n junction (ambipolar), Anisotropic mobility

1. Introduction

Organic semiconductors based on π -conjugated molecules have attracted much attention recently because of their wide potential technological applications, such as organic field-effect transistors (OFETs), organic solar cells (OSCs), organic light-emitting diodes (OLEDs), and various types of chemical sensors [1-3]. Over the past decades, numerous organic semiconductors have extensively investigated experimentally and theoretically due to, for examples, low cost, light weight, ease of processing, versatility of chemical synthesis and flexibility [4]. Among the organic semiconductor investigated, some organic p-type semiconductors have achieved a mobility beyond $10 \text{ cm}^2 \cdot \text{V}^{-1} \cdot \text{s}^{-1}$ [5, 6]. However, the development of the n-type semiconductors significantly lags behind the p-type analogs, which is mainly ascribed to the intrinsic instability of n-type organic materials in air conditions [7]. As a consequence, the search for the high-performance and ambient-stable n-type and/or ambipolar organic materials is a crucial challenge [8].

In the context, we have been searching for new molecules derived from the heterocycles of octathio[8]circulene that can be considered for use as n-type semiconductors using quantum

chemical computations [9]. It is known to all that the π -conjugated molecules such as oligoacenes, oligothiophenes and their derivatives have been widely employed as electron transport materials [10-12]. Based on this, Chernichenko and Nenajdenko *et al.* synthesized a stable, highly symmetric, and planar thiophene-fused[8]annulene, octathio[8]circulene $C_{16}S_8$, named it “sulflower” from sulfur and sunflower [13]. The sulflower molecule with eight π -conjugated annulated thiophene rings is expected to possess the high air-stability. Interestingly, the sulflower molecules in the single crystal display a one dimensional slipped π -stack motif along the crystallographic a-axis with a short interplanar distance of 3.86 Å. This short intermolecular contact provides an efficient charge transport pathway, which renders sulflower a high possibility of three-dimensional transport and thus great potential as a good candidate for the fabrication of organic electronic devices [14–16]. Up to the present, the charge transporting properties of the octathio[8]circulene have been investigated in several experimental and theoretical studies [17]. In this regard, we investigated two novel materials sym-tetraselenatetrathio[8]circulene $C_{16}S_4Se_4$ (selenosulflower) [18] and its selenium analogue $C_{16}Se_8$ (octaseleno[8]circulene, we name it “selflower” from selenium and sunflower) based on the highly symmetric octathio[8]circulene. The two novel compounds were listed in Fig. 1. We performed quantum chemical calculations for the two novel circulenes. The geometries, electronic and charge transport properties, and substituent effects of the two novel circulenes were discussed and analyzed. We hope that our work could be useful to understand how the interplaying role of various factors affects the charge transport property and provide some important information for designing high performance semiconductors.

2. Theoretical methodology and computational details

2.1 Theoretical methodology

At room temperature, the charge transfer in π -conjugated organic semiconductors with weak intermolecular interactions is generally regarded to happen through the incoherent hopping process [19]. Thus, to describe the charge transport properties, the incoherent hopping model was employed in which the charge carriers are expected to localize and jump between neighboring molecules to migrate across the organic layer [20]. The rate of charge transfer between two adjacent molecules, k is expressed by the Marcus equation [21] in terms of the reorganization energy λ , the transfer integral V , and the temperature T as

$$k = \frac{2\pi V^2}{h} \left(\frac{\pi}{\lambda k_B T} \right)^{\frac{1}{2}} \exp\left(-\frac{\lambda}{4k_B T} \right) \quad (1)$$

where h and k_B are the Planck and Boltzmann constants, respectively. The charge transfer mobility, μ , is then evaluated from the Einstein relation [22]

$$\mu = \frac{e}{k_B T} D \quad (2)$$

where e is the electronic charge, and D the diffusion coefficient, which is related to the charge transfer rate k as summing over all the hopping pathways:

$$D = \frac{1}{2n} \sum_i r_i^2 k_i P_i \quad (3)$$

where n is the dimensionally (usually n is equal to 3 in that we could evaluate the average mobility of all the hopping pathways), r_i is the centroid distance of the hopping channel i , and P_i is the relative probability for charge carrier hopping to a particular i th neighbor, which is calculated as by

$$P_i = k_i \left(\sum_i k_i \right)^{-1} \quad (4)$$

The reorganization energy λ has both inner and the external contributions. The inner

reorganization energy is a measure of geometrical distortion of the ionic forms from the neutral molecule [23, 24]. Due to the external part is often neglected, we only considered the inner reorganization energy employing the adiabatic potential (AP) energy surface approach [25]. According to the AP scheme, λ_{\pm} can be expressed as the following equation [26]:

$$\lambda_{\pm} = E_0(Q_{\pm}) - E_0(Q_0) + E_{\pm}(Q_0) - E_{\pm}(Q_{\pm}) \quad (5)$$

where λ_{\pm} is the reorganization energy for hole or electron transports, $E_{\pm}(Q_0)$ is the total energy of a system with positive or negative charge in the optimized neutral geometry, $E_{\pm}(Q_{\pm})$ is the total energy of optimized ionic geometry, and $E_0(Q_0)$ is the total energy of optimized neutral molecule.

The transfer integral V represents the strength of electronic coupling between the two adjacent neighboring molecules. It is calculated on the direct coupling approach, which provides a relatively accurate estimation for the V_i due to considering the spatial overlap between two monomers [27]. In terms of this scheme, the electron coupling is given by

$$V_i = \frac{h_{12} - \frac{1}{2}(h_{11} + h_{22})S_{12}}{1 - S_{12}^2} \quad (6)$$

where $h_{i,j} = \langle \phi_i | h_{KS} | \phi_j \rangle$, $S_{i,j} = \langle \phi_i | S | \phi_j \rangle$, and $|\phi_i\rangle$ ($i=1,2$) is the wave function of the frontier molecular orbital for the i th monomer. h_{ij} is the charge transfer integral and S_{ij} is the spatial overlap integral, respectively. h_{KS} is the Kohn–Sham Hamiltonian of the dimer system, which can be calculated by the following equation [28]: $h_{KS} = SC\varepsilon C^{-1}$, where S is the intermolecular overlap matrix, C and ε are the molecular orbital coefficients and energies from one-step diagonalization without iteration.

One of the most important expected features of the π -conjugated molecules is their abilities to become highly conductive after hole or electron doping. The ionic state properties such as vertical ionization potential (IP_v), adiabatic ionization potential (IP_a), vertical electron affinities (EA_v),

and adiabatic electron affinities (EA_a) were calculated by the following formulas [29]:

$$IP_v / IP_a = E_+(Q_0) / E_+(Q_+) - E_0(Q_0) \quad (7)$$

$$EA_v / EA_a = E_0(Q_0) - E_-(Q_0) / E_-(Q_-) \quad (8)$$

2.2 Computational details

The unit cells of the crystal structure $C_{16}S_4Se_4$ (see Fig. 1) was retrieved from the Cambridge Crystallographic Database ($a=4.029 \text{ \AA}$, $b=16.68 \text{ \AA}$, $c=11.27 \text{ \AA}$, $\alpha=90^\circ$, $\beta=94.30^\circ$, $\gamma=90^\circ$ and $V_{\text{cell}}=709.39 \text{ \AA}^3$). Based on the experimental crystal structure, we performed periodic optimization for $C_{16}S_4Se_4$ crystal by using the dispersion-corrected density functional theory (DFT-D) at the PBE level. Inclusion the dispersion energy (-D) is usually needed to describe the solid-state packing of molecules [30]. The optimized crystal structure parameters were summarized as: $a=3.908 \text{ \AA}$, $b=16.79 \text{ \AA}$, $c=11.30 \text{ \AA}$, $\alpha=90^\circ$, $\beta=94.20^\circ$, $\gamma=90^\circ$ and $V_{\text{cell}}=739.94 \text{ \AA}^3$. It is worth noting that the optimized crystal structure parameters are in good agreement with the experiment, demonstrating that the method is suitable for the molecular crystal. Since sulfur and selenium are in the same group, we substituted all the four sulfur atoms with selenium to obtain a crystal structure of $C_{16}Se_8$ that is similar to $C_{16}S_4Se_4$. In this regard, we also optimized the $C_{16}Se_8$ crystals by DFT-D method with GGA-PBE functionals [31]. The optimized $C_{16}Se_8$ crystal (see Fig. 1) parameters were listed as: $a=4.111 \text{ \AA}$, $b=17.43 \text{ \AA}$, $c=11.85 \text{ \AA}$, $\alpha=90^\circ$, $\beta=95.55^\circ$, $\gamma=90^\circ$ and $V_{\text{cell}}=845.68 \text{ \AA}^3$. All the calculations were performed using the CASTEP code [32].

Large numbers of theoretical studies have shown that the B3P86 functional is recognized to provide reliable predictions and interpretations of the molecular geometries and electronic properties of π -conjugated organic systems bearing sulfur and selenium atoms [18, 33]. Here, all

geometries of the neutral, cationic, and anionic species were optimized using the B3P86 hybrid functional and the 6-31G(d,p) basis set. On the basis of the above calculations, the reorganization energies of the $C_{16}S_4Se_4$ and $C_{16}Se_8$ were obtained. Although the B3LYP functional was widely used, the transfer integral calculated by this functional was overestimated in some cases [18, 34, 35]. In the calculations of the transfer integral, we chose the PW91 exchange and PW91 correlation functionals with 6-31G(d,p) basis set by the site-energy corrected method, which has been proved to give good descriptions for transfer integral at the DFT level [36, 37]. The above calculations were manipulated by the Gaussian 09 package [38].

3. Results and discussion

3.1 Geometric and electronic structures

As seen in Table 1, the optimized bond lengths of $C_{16}S_4Se_4$ are in good agreement with the corresponding experimental values. The largest deviation of the optimized and experiment bond length is only 0.06 Å (R_{10-11}), which is ascribed to the solid state effect in the crystal structure [18]. The results also indicated that the B3P86 functional coupled with the 6-31G(d,p) basis set is appropriate for depicting the geometric properties of the selenosulfur. Judged by the bond lengths and dihedral angles, the optimized selenosulfur and selflower exhibit excellent planarity. The optimized bond lengths of ground, anionic and cationic states of the $C_{16}S_4Se_4$ and $C_{16}Se_8$ molecules at the B3P86/6-31G(d,p) level were listed in Supporting Information. From Table S1 and Table S2, the bond length modifications from neutral to ionized forms in $C_{16}S_4Se_4$ and $C_{16}Se_8$ are ca. of 0.01 Å with the maximum changes of 0.017 Å for $C_{16}S_4Se_4$ and 0.019 Å for $C_{16}Se_8$. This suggested a better structural stability in donating and accepting electrons due to their

special highly conjugated and symmetrical structures [39]. The variations of bond lengths between the neutral, cationic and anionic geometries for $C_{16}S_4Se_4$ and $C_{16}Se_8$ were also presented in Fig. S1 and Fig. S2. As can be seen the geometric deformation of the two molecules in the oxidation process is larger than the reduction process, so the hole reorganization energies for the two molecules should be larger than the corresponding electron ones [40]. To elaborate the geometric distortion quantitatively, we summed up the bond length changes ($\Sigma|\Delta(A-G)|$ and $\Sigma|\Delta(C-G)|$) for the two compounds in charge carrier transport processes [41]. Here $\Delta(A-G)$ represents the bond length difference between the anionic and neutral geometries, $\Delta(C-G)$ denotes the bond length change between the cationic and neutral ones. The calculated $\Sigma|\Delta(A-G)|$ and $\Sigma|\Delta(C-G)|$ values reach 0.244 Å and 0.316 Å for $C_{16}S_4Se_4$ and 0.231 Å and 0.289 Å for $C_{16}Se_8$, respectively. The close values of the bond length changes in charge transfer processes indicate their balanced charge transport property [42]. Further analysis showed that the geometric relaxations of all eight C-S bonds account for 39.3% and 18.2% deformations of $C_{16}S_4Se_4$ in the reduction and oxidation processes, respectively, and those of C-Se bonds reaches 33.7% and 35.5%, respectively. When all the sulfur atoms of $C_{16}S_4Se_4$ are substituted by the selenium atoms, the geometric relaxations from all the peripheral C-Se bonds account for 69.2% and 48.7% deformations of $C_{16}Se_8$, in the reduction and oxidation processes respectively. These results demonstrate that the selenium substitution lead to the smaller geometric modification in the reduction process, which is beneficial to the electron transport of the selfflower crystal.

3.2 Frontier molecular orbitals

The frontier molecular orbitals (FMO) as well as their spatial distribution are the important

factors to illustrate the carrier transport properties [43]. The relative energies of the lowest unoccupied molecular orbitals (LUMOs) and the highest occupied molecular orbitals (HOMOs) provide a reasonable qualitative indication for the electron and hole injection, respectively [44]. The distribution of the FMOs for $C_{16}S_4Se_4$ and $C_{16}Se_8$ were plotted in Fig. 2. The general trend is that the HOMO of the $C_{16}S_4Se_4$ and $C_{16}Se_8$ is predominately composed of delocalized p_z orbitals [45]. Besides, the HOMO and LUMO denote a clearly symmetrical distribution among the two molecules. For the $C_{16}S_4Se_4$, the HOMO is nearly delocalized among the whole molecule except two peripheral selenium atoms, while the HOMO is distributed on the entire molecule for the $C_{16}Se_8$. In addition, the LUMO is mainly delocalized on the peripheral atoms for the $C_{16}S_4Se_4$ and $C_{16}Se_8$. This implies that the position and number of selenium atoms is ascribed to the main reason for the different distribution of the HOMOs and LUMOs [46]. The values of the energies of LUMOs and HOMOs of the two molecules were presented in Table 2. It can be found that by replacing the sulfur atoms with the selenium, the energy of the HOMO increases and the energy of the LUMO decreases slightly due to the energy of the p -orbitals increase. With reference to conductivity, the energy difference between the HOMO and LUMO (E_{gap}) can be considered approximately as the band gap energy [45]. The E_{gap} of the $C_{16}Se_8$ is obviously less than the E_{gap} of the $C_{16}S_4Se_4$ (Table 2), which indicates that the $C_{16}Se_8$ is slightly more conductive. Hence one can see that the replacement of the peripheral sulfur atoms by the selenium atoms will cause the significant changes in the distribution and energy levels of the FMOs, which will further influence the charge transport properties.

3.3 Electron affinity, ionization potential and reorganization energy

The molecular electron affinity (EA) and ionization potential (IP) are the most important parameters to characterize the ability of the charge injection [47]. To inject an electron into the LUMO efficiently, EA must be high enough, which is an important requirement of an excellent n-type organic semiconductor. On the contrary, IP must be low enough to allow an efficient hole injection into the HOMO [48, 49]. According to Equations 7 and 8, the values of EA and IP for the $C_{16}S_4Se_4$ and $C_{16}Se_8$ at the B3P86/6-31G(d,p) level, for both vertical and adiabatic ones, were summarized in Table 3. Liu and Mao *et al.* have reported that the adiabatic potential (IP_a) of p-type transport materials which are stable in air ranges from 5.680 eV to 6.786 eV [50], while the IP_a of the $C_{16}S_4Se_4$ is 6.753 eV and it has a lower electronic affinity value of 0.229 and 0.193 eV for vertical and adiabatic excitations, respectively. In the viewpoint of ionization potential, the $C_{16}S_4Se_4$ is more suitable for p-type material. In contrary, the $C_{16}Se_8$ has a larger vertical electron affinity (0.445 eV) and larger IP_V (7.284 eV), which suggests that the $C_{16}Se_8$ is more suitable for n-type though it has an ambipolar mobility. A larger EA_V value ensures that the radical anion of the $C_{16}Se_8$ has a high stability in ambient atmosphere [51]. The above investigations show that the attachment of selenium atoms to the peripheral thiophene ring can significantly influence the ability of electron-accepting of selenosulfur molecule.

Reorganization energy (λ) is one of the important factors governing the charge mobilities of the organic semiconductors. For efficient charge transfer, the reorganization energy should be smaller. The reorganization energies are in proportion to the deformation of the geometries in charge transfer process [52]. The reorganization energies of hole and electron transport of $C_{16}S_4Se_4$ and $C_{16}Se_8$ were obtained through the adiabatic potential (AP) energy surface approach at the B3P86/6-31G(d,p) level. All the reorganization energies of the two compounds were listed

in Table 3. The magnitude of the hole reorganization energy (λ_h) for each molecule is profoundly larger than its corresponding electron reorganization energy (λ_e), which indicates that they could be good electron transport materials. For isolated molecules, the λ_h and λ_e of the $C_{16}S_4Se_4$ are somewhat larger than the corresponding λ_h and λ_e of the $C_{16}Se_8$, indicating that a possibility in the improvement of hole and electron transfer as the sulfur atoms were substituted by the selenium atoms. The evolutionary trends of λ_h and λ_e could be explained in terms of the geometry changing when the electronic state changes. As is clearly visible from the Fig. S1 and Fig. S2 (Supporting Information), the $C_{16}S_4Se_4$ has a large λ_h due to a marked deviation from planar geometry as the hole injection may be subjected to the alternately located S/Se atoms in its periphery. Besides, the relatively small λ_e of the $C_{16}Se_8$ can be reasoned for there is no profound torsion of the anionic structure compared to the planar neutral structure. The λ_e of the $C_{16}Se_8$ is only 61 meV, which is much smaller than that of C_{60} (132 meV) [53], a widely used n-type material. From the reorganization energy, the $C_{16}Se_8$ is more suitable for the n-type material and has relatively large electron mobility. The above results indicate that the electron reorganization becomes small with sulfur atoms being substituted by selenium atoms, which will improve the mobility of the charge transport.

3.4 Transfer integral

The transfer integrals are very sensitive to the relative position of interacting molecules in the crystals and are dependent on the molecular packing manner [54]. For different crystal structures, the relative positions of the two neighboring molecules involved are entirely different due to different packing structures in crystals. Among these hopping channels, two common hopping

channels adopted can yield strong intermolecular interactions to promote charge transport. One is face-to-edge packing yielding two-dimensional interaction in crystals. The other is face-to-face packing (π - π stacking), typically with some degree of displacement along the short axes of the molecules [55, 56]. For the crystals of the $C_{16}S_4Se_4$ and $C_{16}Se_8$, the main charge transfer pathways were illustrated in Fig. 3 and Fig. 4. It is worth to notice that both the $C_{16}S_4Se_4$ and $C_{16}Se_8$ have rigorous plane structure and mainly employ the π - π stacking configurations, but in different transfer pathways. The displacements of the dimers along the long-axis and the short-axis as well as the vertical distances are different. The transfer integral of each pathway was calculated at the PW91PW91/6-31G (d,p) level by the site-energy corrected method and the corresponding results were listed in Table 4. It is generally accepted that the transfer integral between the neighboring molecules is closely related to the intermolecular interactions [46]. As shown in Table 4, for the $C_{16}S_4Se_4$ and $C_{16}Se_8$, since both the calculated reorganization energies of hole and electron transport are larger than the largest hole and electron transfer integral, the localized description of the charge transfer by the Marcus–Hush model is adequate for investigating the charge mobilities of the two compounds [42]. It is noticed that the electron transfer integral in various hopping pathways are remarkably different. For the $C_{16}S_4Se_4$, the electronic couplings along the short-axis (dimers P1 and P2) are larger than other directions, which means that electrons transfer mainly along one-dimension. The same transport properties can also be found in $C_{16}Se_8$, the electronic couplings along the short-axis (dimers P1 and P2) are 54.51 meV, more than 5 fold of those along other directions, demonstrating that the electron mobility of each crystal is mainly determined by one dimensional charge transport. Furthermore, for both $C_{16}S_4Se_4$ and $C_{16}Se_8$, the transfer integrals for electron and hole have profound difference among the dimers P1, P3 and P11. The

transfer integrals of in dimer P1 are larger or much larger than those of dimers P3 and P11 since there is a face to face π - π orbital interaction in dimer P1. The differences of transfer integrals in dimers P3 and P11 can be interpreted by the contours of their HOMO and LUMO. As shown in Fig. 5, for example, the atomic orbitals in the intermolecular contacting region contributes more to its LUMO than those outside the region, resulting in a large electron transport integral (V_e) in dimer P3 of $C_{16}Se_8$. While in dimer P11, there is even an overlap between the LUMOs of their respective monomer, making its V_e value more than twice that of dimer P3. On the contrary, the atomic orbitals in the intermolecular contacting region contributes less to its HOMO as compared to LUMO, which means a less contributions from the atomic orbitals in the intermolecular contacting region and thus a small hole transport integral (V_h) for both dimers of P3 and P11. Interestingly, in comparison with $C_{16}S_4Se_4$, the largest electron transfer integral of the $C_{16}Se_8$ (54.15 meV) is obviously larger than the largest V_e of the $C_{16}S_4Se_4$ (23.80 meV), which can be attributed to the easily polarizable of selenium atoms. As a result, the $C_{16}Se_8$ is more suitable to be electron transport material. In general, the electron transfer along π - π stacking is crucial to the charge mobility and the substitution of the selenium atoms can significantly change the transfer integral.

3.5 Charge carrier mobility and anisotropic mobility

The reorganization energy and charge transfer integral are used to calculate the charge mobilities for the $C_{16}S_4Se_4$ and $C_{16}Se_8$ based on Equations 1, 2 and 6. The calculated hole and electron mobilities of the two compounds were summarized in Table 5. In comparison with previous research [15], it is noted that there is a large difference in the mobilities between previous

and our works. Some investigations demonstrated that the organic thin film transistor measurements of mobility are varied a lot when the substrate is modified or the temperature is changed. Dadvand *et al.* fabricated a thin-film OFET of selenosulfur using Au electrodes and an SiO₂ gate with the resultant hole mobility of about $1 \times 10^{-3} \text{ cm}^2 \cdot \text{V}^{-1} \cdot \text{s}^{-1}$ [15], while our theoretical charge transport investigation is under the ideal conditions of perfect crystal at room temperature. Theoretical works provide an upper limit of the charge mobility, and thus usually overestimates. The experimental mobility is very sensitive to the experimental conditions. Film of the selenosulfur demonstrates a different growth mode compared to other organic materials. No substantial growth of the grains for the C₁₆S₄Se₄ results in a large number of grain boundaries and negatively affects the charge mobility [15]. The unfavorable growth is caused by the very low energy of molecule-surface interactions, which often attributed to that the organic semiconductor material has the small mobility. Some other possible reasons attributed to the discrepancy involve the influence of carrier trap, energy traps and grain boundary in experiments, the approximation of Marcus theory formulation for hopping rate in theory [57]. Despite of more or less differences between theory and experiment, the calculated results could provide the reasonable expectations and assist to understand the detailed transport behaviors of charge carriers. As a whole, the electron mobilities are larger than the hole mobilities for both the C₁₆S₄Se₄ and C₁₆Se₈, indicating that both compounds are more suitable for n-type materials than for p-type. In addition, the calculated mobilities of the C₁₆S₄Se₄ and C₁₆Se₈ are much more than $0.1 \text{ cm}^2 \cdot \text{V}^{-1} \cdot \text{s}^{-1}$, a threshold that fully meets the practical OFET application [58], especially the C₁₆Se₈ demonstrated excellent electron-dominated ambipolar performance [59, 60], with electron and hole mobilities reaching as large as 1.26 and 1.03 $\text{cm}^2 \cdot \text{V}^{-1} \cdot \text{s}^{-1}$, respectively. The large electron conductance of C₁₆Se₈ crystal

is primarily due to its relatively smaller electron reorganization energy and larger electron transfer integral. Apparently, when the sulfur atom is substituted by selenium atom, both hole and electron mobilities of $C_{16}Se_8$ increase, especially the electron mobility that is almost two fold larger than the corresponding electron mobility of $C_{16}S_4Se_4$ ($0.74 \text{ cm}^2 \cdot \text{V}^{-1} \cdot \text{s}^{-1}$). The investigation on the intrinsic transport properties aims to guide the design of novel functional materials. Organic crystals like the selfflower would provide better efficiency for electronic devices.

As is known to all, the strong thermal molecular motions may cause dynamic disorder of molecular disorientation in the crystal structures at the high temperature, which may enhance the fluctuation in the intermolecular transfer integrals [61, 62]. As can be seen in Table 5, we speculated that the charge transports in the $C_{16}S_4Se_4$ and $C_{16}Se_8$ crystals are remarkably anisotropic. As a result, we have investigated the anisotropic effect in the $C_{16}S_4Se_4$ and $C_{16}Se_8$ to understand how it influences the charge mobility. The angular resolution anisotropic mobility can be calculated by the following equation [12]:

$$\mu_{\Phi} = \frac{e}{2k_B T} \sum_i r_i^2 k_i P_i \cos^2 \gamma_i \cos^2(\theta_i - \Phi) \quad (9)$$

where Φ is the orientation angle of the transistor channel relative to the reference crystallographic axis, and θ_i is the angle of the projected hopping paths of different dimers relative to the reference axis. We only considered the dimer P (P1) in the mobility orientation function on the basal stacked layer due to the smaller transfer integrals along the dimer T1 (P11) and dimer T2 (P13) transfer pathways in the $C_{16}S_4Se_4$ and $C_{16}Se_8$, that is, $\gamma_i = 0^\circ$. Fig. 6 and Fig. 7 described the angular-resolution anisotropic mobilities of both electron and hole transports of $C_{16}S_4Se_4$ and $C_{16}Se_8$. The $C_{16}S_4Se_4$ and $C_{16}Se_8$ crystals exhibit remarkable anisotropic charge-transporting behaviors. At the reference angles of 0° and 180° , maxima hole mobility were found (0.725

$\text{cm}^2 \cdot \text{V}^{-1} \cdot \text{s}^{-1}$ for $\text{C}_{16}\text{S}_4\text{Se}_4$ and $1.521 \text{ cm}^2 \cdot \text{V}^{-1} \cdot \text{s}^{-1}$ for C_{16}Se_8), corresponding to the transport pathways with π - π intermolecular interactions. On the contrary, the minima appear along the b -axis direction, which corresponds to the reference angle of close 90° and 270° . However, unlike the hole mobility, the electron mobility shows completely different transport character in the $\text{C}_{16}\text{S}_4\text{Se}_4$ and C_{16}Se_8 crystals. For the $\text{C}_{16}\text{S}_4\text{Se}_4$, the electron mobility is obvious anisotropic, while in the C_{16}Se_8 crystal, the anisotropic behavior is not profound, which attributed to the large uniform electronic couplings in the dimers P, T1 and T2, so a relatively balanced charge transport is observed along any direction in the selected a - b plane. For the electron transport of the $\text{C}_{16}\text{S}_4\text{Se}_4$, the largest electron mobility ($0.625 \text{ cm}^2 \cdot \text{V}^{-1} \cdot \text{s}^{-1}$) is along or near the 0° and 180° directions relative to the a axis. In addition, the C_{16}Se_8 has the highest angular electron mobility ($1.31 \text{ cm}^2 \cdot \text{V}^{-1} \cdot \text{s}^{-1}$) at the reference angle of 13° and 193° (a slight deviation from 0° to 180°), the directions of the smallest mobility is perpendicular to the axis mentioned above in the selected planes, indicating that the electronic coupling of LUMOs is the strongest along the shortest distance between two monomers (along the P direction). Additionally, for the $\text{C}_{16}\text{S}_4\text{Se}_4$, the electron transfer integral for the dimers P and T2 are of the same magnitude, so the anisotropic electron mobilities are influenced by these two pathways according to Equation 9. The hole transfer integral for the dimer P is remarkably larger than dimers T1 and T2. The dimer P with π - π interactions are the main driving force of the anisotropic hole mobilities.

3.6 Band structure

In order to have an in-depth understanding of the anisotropy of charge transport in single crystals, the band structures of $\text{C}_{16}\text{S}_4\text{Se}_4$ and C_{16}Se_8 , which could expand the charge transport to

the whole multidimensional space, are examined and depicted in Fig. 8. It can be seen that both valence bands (VBs) and conduction bands (CBs) consist of two subbands due to two inequivalent molecules existing in the primitive cells of $C_{16}S_4Se_4$ and $C_{16}Se_8$. In general, the appearance of both dispersive and flat bands is a reflection of anisotropy in the charge transport properties of the crystal. And the stronger dispersion of band is, the larger carrier mobility is [63]. As shown in Fig. 8, for $C_{16}S_4Se_4$, the strongest conduction dispersion occurs in the GY subzone, corresponding to the a axis in real space. Besides, the dimers P1 and P2 with the maximal electron coupling are along this direction. The biggest dispersion in valence band (VB) along the GY direction is smaller than that in conduct band (CB), which further indicates that the crystal of $C_{16}S_4Se_4$ has better electron transport properties. Compared to $C_{16}S_4Se_4$, the $C_{16}Se_8$ has stronger dispersions in CB and VB, which demonstrates that it has excellent carrier transport performance, and the strongest dispersions in CB and VB correspond to the π - π packing direction which shows the paths with large transfer integral are along the direction with strong dispersions. In addition, the biggest dispersion in CB is broader than that in VB, suggesting that the electron transfer ability is superior to the hole one. Furthermore, the band gap of the $C_{16}S_4Se_4$ (2.292 eV) is larger than its selenium analogue “selflower” $C_{16}Se_8$ (2.279 eV) since the selenium atoms with large polarizability are generally expected to provide for stronger interactions. In a word, introducing the more selenium atoms to the peripheral thiophene ring of the $C_{16}S_4Se_4$ can increase the hole and electron mobilities, which are consistent with the conclusions obtained from the hopping model discussed above.

4. Conclusion

The geometrical and crystal structures, electronic properties and charge mobilities of selenosulfur and selflower as organic semiconductors have been investigated using DFT methods coupled with the charge-hopping mechanism. The investigation indicates that the $C_{16}Se_8$ with low-lying and delocalized LUMOs and relatively large adiabatic electron affinities can easily function as electron-dominated ambipolar organic semiconductor. The results reveal that the reorganization energy and the transfer integral have been influenced by the substitution of sulfur atoms with selenium atoms, which induced an increase of the charge mobility. The smaller reorganization energy and the larger electron transfer of $C_{16}Se_8$ enabled it to have the largest electron mobility ($1.26 \text{ cm}^2 \cdot \text{V}^{-1} \cdot \text{s}^{-1}$). Both hole and electron mobilities of $C_{16}Se_8$ exceed $1 \text{ cm}^2 \cdot \text{V}^{-1} \cdot \text{s}^{-1}$, which denotes that the $C_{16}Se_8$ single crystal may be an ideal candidate as high performance ambipolar organic semiconductor material. The transfer integral calculations among the dominant hopping pathways show that the charge transport processes occur in parallel π - π stacking dimers for both $C_{16}S_4Se_4$ and $C_{16}Se_8$. Additionally, the band structure calculations suggested that the dimer with π - π stacking with larger transfer integral were along the direction with dispersions in VB and CB. Besides, $C_{16}S_4Se_4$ and $C_{16}Se_8$ crystals exhibit remarkable anisotropic charge transport behaviors and the maximal charge mobility is along a special crystal axis direction. Our investigations revealed that the selflower with large carrier mobilities have potential applications as high performance electron-dominated ambipolar organic semiconductors.

Acknowledgements

The authors thank the National Science Foundation of China (No. 21372116) as well as the Project Funded by the Priority Academic Program Development of Jiangsu Higher Education

Institutions (PAPD) for supporting this work.

References

- [1] R. Chesterfield, C. Newman, T. Pappenfus, P. Ewbank, K. Haukaas, K. Mann, L. Miller and C. Frisbie, *Adv. Mater.*, 2003, **15**, 1278–1282.
- [2] M. E. Gershenson, V. Podzorov and A. F. Morpurgo, *Rev. Mod. Phys.*, 2006, **78**, 973–989.
- [3] X. W. Zhan, A. Facchetti, S. Barlow, T. J. Marks, M. A. Ratner, M. R. Wasielewski and S. R. Marder, *Adv. Mater.*, 2011, **23**, 268–284.
- [4] B. Kippelen and J. -L. Brédas, *Energy Environ. Sci.*, 2009, **2**, 251–261.
- [5] V. C. Sundar, J. Zaumseil, V. Podzorov, E. Menard, R. L. Willett, M. E. Gershenson and J. A. Rogers, *Science*, 2004, **303**, 1644–1646.
- [6] V. Podzorov, E. Menard, A. Borissov, V. Kiryukhin, J. A. Rogers and M. E. Gershenson, *Phys. Rev. Lett.*, 2004, **93**, 086602.
- [7] Z. Bao, *Adv. Mater.*, 2002, **12**, 227–230.
- [8] X. Wang and K. -C. Lau, *J. Phys. Chem. C*, 2012, **116**, 22749–22758.
- [9] A. Datta and K. P. Swapan, *J. Phys. Chem. C*, 2007, **111**, 4487–4490.
- [10] L. Torsi, A. Dodabalapur, L. J. Rothberg, A. W. Fung and H. E. Katz, *Phys. Rev. B*, 1998, **57**, 2271–2275.
- [11] W. Q. Deng and W. A. Goddard III, *J. Phys. Chem. B*, 2004, **108**, 8614–8621.
- [12] S. H. Wen, A. Li, J. Song, W. Q. Deng, K. L. Han and W. A. Goddard III, *J. Phys. Chem. B*, 2009, **113**, 8813–8819.
- [13] K. Y. Chernichenko, V. V. Sumerin, R. V. Shpanchenko, E. S. Balenkova and V. G.

- Nenajdenko, *Angew. Chem. Int. Ed.*, 2006, **45**, 7367–7370.
- [14] G. Godefroid and J. -P. Zhang, *Phys. Chem. Chem. Phys.*, 2008, **10**, 1743–1747.
- [15] A. Dadvand, F. Cicoira, K. Y. Chernichenko, E. S. Balenkova, R. M. Osuma, F. Rosei, V. G. Nenajdenko and D. F. Perepichka, *Chem. Commun.*, 2008, 5354–5356.
- [16] T. Fujimotor, M. M. Matsushita and K. Awaga, *Appl. Phys. Lett.*, 2010, **97**, 14832–14841.
- [17] W. D. Xiao, Y. Y. Zhang, L. Tao, K. Ait-Mansour, K. Y. Chernichenko, V. G. Nenajdenko, P. Ruffieux, S. X. Du, H.-J. Gao and R. Fasel, *Scientific Reports*, 4, 5415.
- [18] G. Godefroid, J. -P. Zhang and T. Barancira, *J. Phys. Chem. A*, 2009, **113**, 255–262.
- [19] Z. G. Shuai, L. Wang and Q. Li, *Adv. Mater.*, 2011, **23**, 1145–1153.
- [20] J. Cornil, J. -L. Brédas, J. Zaumseil and H. Sirringhaus, *Adv. Mater.*, 2007, **19**, 1791–1799.
- [21] R. A. Marcus, *Rev. Mod. Phys.*, 1993, **65**, 599–610.
- [22] J. Cornil, V. Lemaire, J. P. Calbert and J. -L. Brédas, *Adv. Mater.*, 2002, **14**, 726–729.
- [23] B. S. Brunshwig, J. Logan, M. D. Newton and N. Sutin, *J. Am. Chem. Soc.*, 1980, **102**, 5798–5809.
- [24] M. D. Newton and N. Sutin, *Ann. Rev. Phys. Chem.*, 1984, **35**, 437–480.
- [25] M. Malagoli and J. -L. Brédas, *Chem. Phys. Lett.*, 2000, **327**, 13–17.
- [26] M. X. Zhang, S. Chai and G. J. Zhao, *Org. Electron.*, 2012, **13**, 215–221.
- [27] E. F. Valeev, V. Coropceanu, D. A. da Silva Filho, S. Salman and J. -L. Brédas, *J. Am. Chem. Soc.*, 2006, **128**, 9882–9886.
- [28] S. W. Yin, Y. P. Yi, Q. X. Li, G. Yu, Y. Q. Liu and Z. G. Shuai, *J. Phys. Chem. A*, 2006, **110**, 7138–7143.
- [29] L. J. Wang, P. Li, B. Xu, H. Y. Zhang and W. J. Tian, *Org. Electron.*, 2014, **15**, 2476–2485.

- [30] J. C. Sancho-Garcia, A. J. Perez-Jimenez, Y. Olivier and J. Cornil, *Phys. Chem. Chem. Phys.*, 2010, **12**, 9381–9388.
- [31] J. P. Perdew, K. Burke and M. Ernzerhof, *Phys. Rev. Lett.*, 1996, **77**, 3865–3868.
- [32] S. J. Clark, M. D. Segall, C. J. Pickard, P. J. Hasnip, M. I. Probert, K. Refson and M. C. Payne, *Z. Kristallogr.*, 2005, **220**, 567.
- [33] S. Chai, S. H. Wen, J. D. Huang and K. L. Han, *J. Comput. Chem.*, 2011, 3218–3225.
- [34] G. Godefroid, B. Zhang and J. -P. Zhang, *J. Phys. Chem. C*, 2007, **111**, 4838–4846.
- [35] T. Fujimoto, R. Suizu, H. Yoshikawa and K. Awaga, *Chem. Eur. J.*, 2008, **14**, 6053–6056.
- [36] A. Troisi and G. Orlandi, *Chem. Phys. Lett.*, 2001, **344**, 509–518.
- [37] G. Nan and Z. Li, *Org. Electron.*, 2012, **13**, 1229–1236.
- [38] M. J. Frisch, G. W. Trucks, H. B. Schlegel, G. E. Scuseria, M. A. Robb, J. R. Cheeseman, G. Scalmani, V. Barone, B. Mennucci, G. A. Petersson, H. Nakatsuji, M. Caricato, X. Li, H. P. Hratchian, A. F. Izmaylov, J. Bloino, G. Zheng, J. L. Sonnenberg, M. Hada, M. Ehara, K. Toyota, R. Fukuda, J. Hasegawa, M. Ishida, T. Nakajima, Y. Honda, O. Kitao, H. Nakai, T. Vreven, J. A. Montgomery, Jr., J. E. Peralta, F. Ogliaro, M. Bearpark, J. J. Heyd, E. Brothers, K. N. Kudin, V. N. Staroverov, R. Kobayashi, J. Normand, K. Raghavachari, A. Rendell, J. C. Burant, S. S. Iyengar, J. Tomasi, M. Cossi, N. Rega, J. M. Millam, M. Klene, J. E. Knox, J. B. Cross, V. Bakken, C. Adamo, J. Jaramillo, R. Gomperts, R. E. Stratmann, O. Yazyev, A. J. Austin, R. Cammi, C. Pomelli, J. W. Ochterski, R. L. Martin, K. Morokuma, V. G. Zakrzewski, G. A. Voth, P. Salvador, J. J. Dannenberg, S. Dapprich, A. D. Daniels, O. Farkas, J. B. Foresman, J. V. Ortiz, J. Cioslowski, and D. J. Fox, Gaussian, Inc., Wallingford CT, 2009.

- [39] G. V. Baryshnikov, B. F. Minaev, V. A. Minaeva and V. G. Nenajdenko, *J. Mol. Model.*, 2013, **19**, 4511–4519.
- [40] X. K. Chen, J. F. Guo, L. Y. Zou, A. M. Ren and J. X. Fan, *J. Phys. Chem. C*, 2011, **115**, 21416–21428.
- [41] C. B. Zhao, Y. L. Guo, L. Guan, H. G. Ge, S. W. Yin and W. L. Wang, *Syn. Metals.*, 2014, **188**, 146–155.
- [42] C. B. Zhao, W. L. Wang, S. W. Yin and Y. Ma, *New J. Chem.*, 2013, **37**, 2925–2934.
- [43] S. F. Zhang, X. K. Chen, J. X. Fan and A. M. Ren, *Org. Electron.*, 2013, **14**, 607–620.
- [44] L. L. Lin, H. Geng, Z. G. Shuai and Y. Luo, *Org. Electron.*, 2012, **13**, 2763–2772.
- [45] B. Napolion, F. Hagelberg, M. J. Huang, J. D. Watts, T. M. Simeon, D. Vereen, W. L. Walters and Q. L. Williams, *J. Phys. Chem. A*, 2011, **115**, 8682–8690.
- [46] X. D. Tang, Y. Liao, H. Z. Gao, Y. Geng and Z. M. Su, *J. Mater. Chem.*, 2012, **22**, 6907–6918.
- [47] G. Saranya, K. Navamani and K. Senthilkumar, *Chem. Phys.*, 2014, **433**, 48–59.
- [48] H. G. Liu, J. L. Mu and J. -Y. Lee, *J. Phys. Chem. B*, 2011, **115**, 8409–8416.
- [49] J. E. Norton and J. -L. Brédas, *J. Am. Chem. Soc.*, 2008, **130**, 12377.
- [50] C. C. Liu, S. W. Mao and M. Y. Kuo, *J. Phys. Chem. C*, 2010, **114**, 22316–22321.
- [51] Y. C. Chang, M. Y. Kuo, C. P. Chen, H. F. Lu and I. Chao, *J. Phys. Chem. C*, 2010, **114**, 11595–11601.
- [52] S. T. Bromley, M. M. Torrent, P. Hadley and C. Rovira, *J. Am. Chem. Soc.*, 2004, **126**, 6544–6545.
- [53] A. Datta, S. Mohakud and S. -K. Pati, *J. Mater. Chem.*, 2007, **17**, 1933–1938.

- [54] W. Wu, Y. Liu and D. B. Zhu, *Chem. Soc. Rev.*, 2010, **39**, 1489–1502.
- [55] F. Otón, R. Pfattner, E. Pavlica, Y. Oliver, J. Veciana and C. Rovira, *Chem. Mater.*, 2011, **23**, 851–861.
- [56] J. E. Anthony, *Chem. Rev.*, 2006, **106**, 5028–5048.
- [57] B. Zhang, Y. H. Kan, Y. Geng, Y. A. Duan, H. B. Li, J. Hua and Z. M. Su, *Org. Electron.*, 2013, **14**, 1359–1369.
- [58] H. Usta and A. Facchetti, *Acc. Chem. Res.*, 2011, **44**, 501–510.
- [59] Y. Zhao, Y. L. Guo and Y. Q. Liu, *Adv. Mater.*, 2013, **25**, 5372–5391.
- [60] L. J. Wang, G. J. Nan, X. D. Yang, Q. Peng, Q. K. Li and Z. G. Shuai, *Chem. Soc. Rev.*, 2010, **39**, 423–434.
- [61] Y. Geng, H. B. Li, S. X. Wu and Z. M. Su, *J. Mater. Chem.*, 2012, **22**, 20840–20851.
- [62] L. Wang, Q. Li, Z. G. Shuai, L. Chen and Q. Shi, *Phys. Chem. Chem. Phys.*, 2010, **12**, 3309–3314.
- [63] Y. A. Duan, H. B. Li, Y. Geng, Y. Wu, G. Y. Wang and Z. M. Su, *Org. Electron.*, 2014, **15**, 602–613.

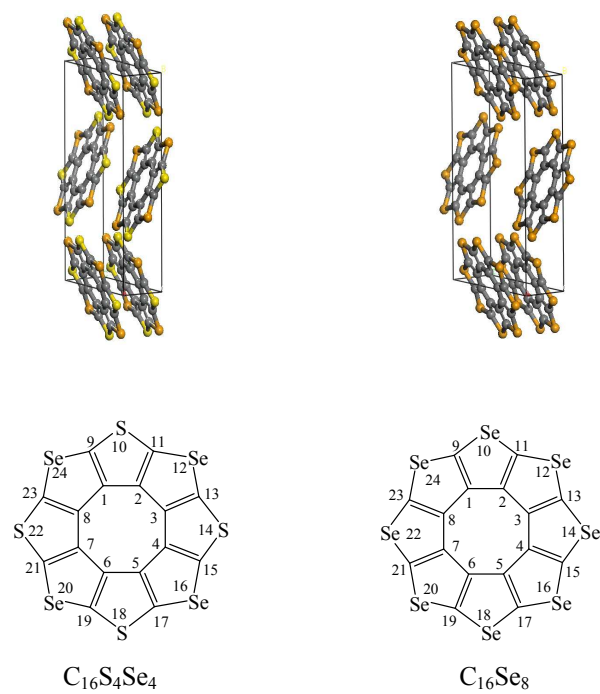


Fig. 1 Crystal (up) and molecular (below) structures of $C_{16}S_4Se_4$ (left) and $C_{16}Se_8$ (right).

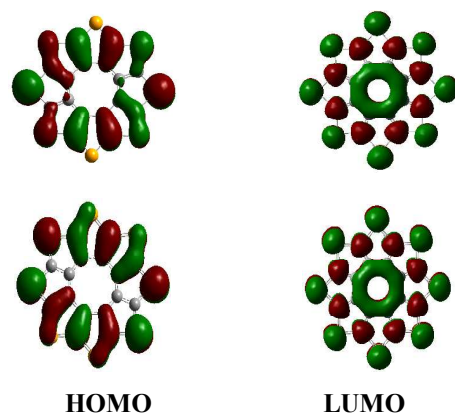


Fig. 2 Distribution of HOMOs and LUMOs of $C_{16}S_4Se_4$ (up) and $C_{16}Se_8$ (below) at the B3P86/6-31G (d,p) level.

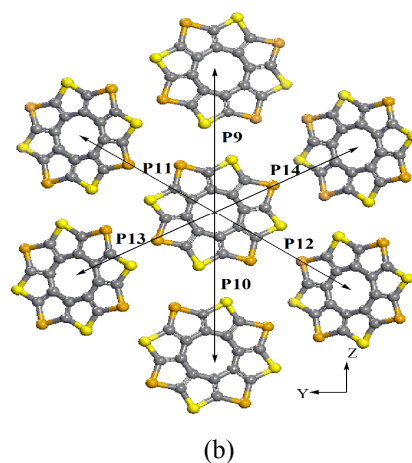
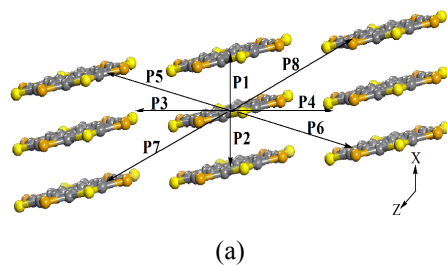


Fig. 3 Charge hopping pathways schemes for the $C_{16}S_4Se_4$; (a) short-axis view and (b) long-axis view of the $C_{16}S_4Se_4$.

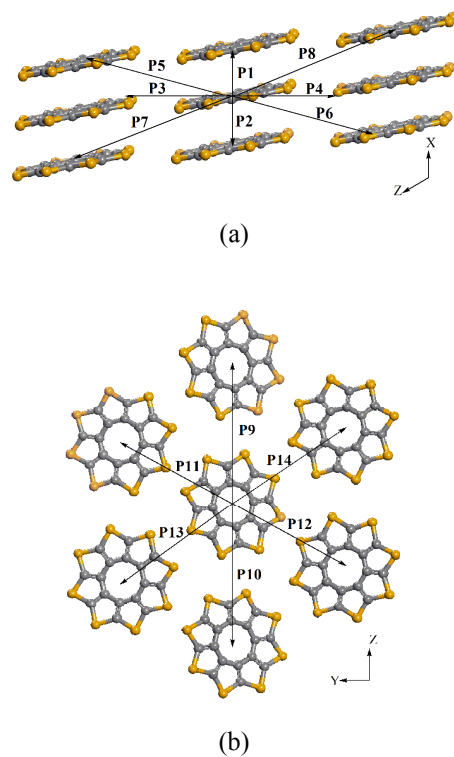


Fig. 4 Charge hopping pathways schemes for the $C_{16}Se_8$; (a) short-axis view and (b) long-axis view of the $C_{16}Se_8$.

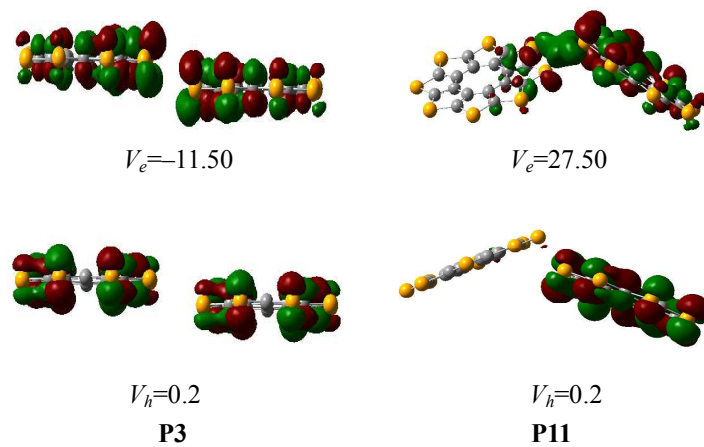


Fig. 5 Orbital interaction and transfer integrals (in meV) of dimers P3 (left) and P11 (right) in the $C_{16}Se_8$ crystal.

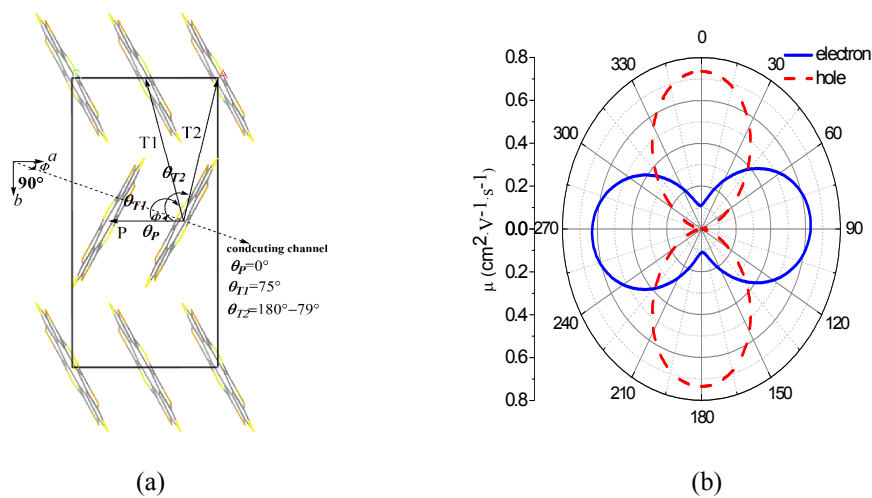


Fig. 6 (a) Illustration of projecting different hopping pathways onto a transistor channel in a - b plane of the $C_{16}S_4Se_4$ crystals; θ_P , θ_{T1} and θ_{T2} are the angles of P, T1 and T2 dimers relative to the reference crystallographic axis a . Φ is the angle along a transistor channel relative to the reference crystallographic axis a . (b) The predicted anisotropic electronic (blue) and hole (red) mobility on the a - b plane of the $C_{16}S_4Se_4$ crystal.

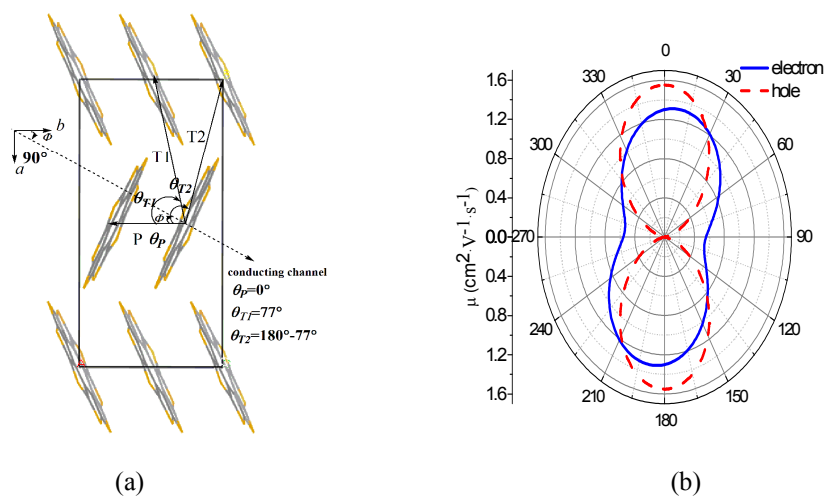


Fig. 7 (a) Illustration of projecting different hopping pathways onto a transistor channel in a - b plane of the $C_{16}Se_8$ crystals; θ_P , θ_{T1} and θ_{T2} are the angles of P, T1 and T2 dimers relative to the reference crystallographic axis b . Φ is the angle along a transistor channel relative to the reference crystallographic axis b . (b) The predicted anisotropic electronic (blue) and hole (red) mobility on the a - b plane of the $C_{16}Se_8$ crystal.

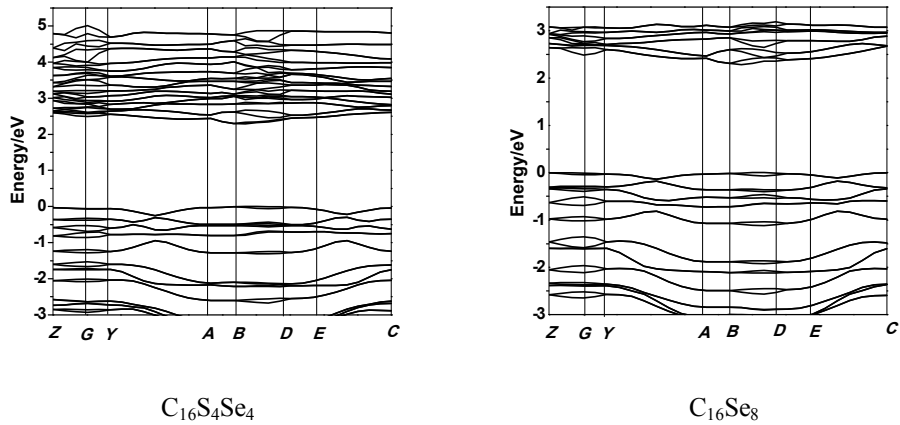


Fig. 8 Illustration of the energy band structures of $C_{16}S_4Se_4$ and $C_{16}Se_8$ crystals.

Table 1 Comparison of optimized bond lengths (in Å), dihedral angles (in °) and experimental values of $C_{16}S_4Se_4$ and $C_{16}Se_8$ at the B3P86/6-31G (d,p) level ^a

Compound	Bond or dihedral angle			
$C_{16}S_4Se_4$	R_{1-2}	1.429 (1.449)	R_{2-3}	1.431 (1.452)
	R_{1-9}	1.383 (1.385)	R_{2-11}	1.383 (1.355)
	R_{9-10}	1.737 (1.793)	R_{11-12}	1.870 (1.865)
	R_{10-11}	1.737 (1.798)	R_{12-13}	1.870 (1.866)
	$D_{9-1-2-11}$	-0.001 (0.82)	$D_{2-1-9-24}$	180.03 (-179.60)
	$D_{8-1-2-21}$	-179.98 (178.89)	$D_{2-1-8-23}$	179.95 (178.73)
$C_{16}Se_8$	R_{1-2}	1.442	R_{9-10}	1.853
	R_{1-9}	1.385	R_{10-11}	1.853
	$D_{9-1-2-11}$	-0.024	$D_{8-1-2-21}$	179.984

^a Data in parenthesis are the average experimental values based on the X-ray structure from CCDC No.707828.

Table 2 The energies of LUMOs and HOMOs (in eV) of the C₁₆S₄Se₄ and C₁₆S₈ with the method B3P86/6-31G (d,p)

Compound	E_{HOMO}	E_{LUMO}	$E_{\text{gap}}^{\text{a}}$
C ₁₆ S ₄ Se ₄	-6.19	-1.66	4.54
C ₁₆ Se ₈	-6.01	-1.73	4.27

^a $E_{\text{gap}} = E_{\text{LUMO}} - E_{\text{HOMO}}$

Table 3 Calculated ionization potentials (IP), electron affinities (EA) and reorganization energies (λ_h and λ_e) for the $C_{16}S_4Se_4$ and $C_{16}Se_8$ at the B3P86/6-31G(d,p) level (in eV)

Compound	IP_V	IP_a	EA_V	EA_a	λ_h	λ_e
$C_{16}S_4Se_4$	6.814	6.753	0.229	0.193	0.117	0.072
$C_{16}Se_8$	7.284	7.230	0.445	0.475	0.109	0.061

Table 4 The transfer integrals for different molecular pairs in the $C_{16}S_4Se_4$ and $C_{16}Se_8$ crystals

Compound	Pathways	r^a	V_e^b	V_h^b
$C_{16}S_4Se_4$	P1 and P2	4.03	23.80	-54.70
	P3 and P4	11.27	-20.70	-0.70
	P5 and P6	11.68	9.00	5.10
	P7 and P8	12.25	9.40	-5.80
	P9 and P10	11.27	-20.70	-0.70
	P11 and P12	10.35	0.70	-0.60
	P13 and P14	10.18	21.50	-7.80
$C_{16}Se_8$	P1 and P2	3.87	54.51	73.61
	P3 and P4	11.14	-11.50	0.20
	P5 and P6	11.53	7.10	-4.40
	P7 and P8	12.04	4.90	1.10
	P9 and P10	11.14	-11.50	0.20
	P11 and P12	10.07	27.50	0.20
	P13 and P14	10.22	-13.80	-3.60

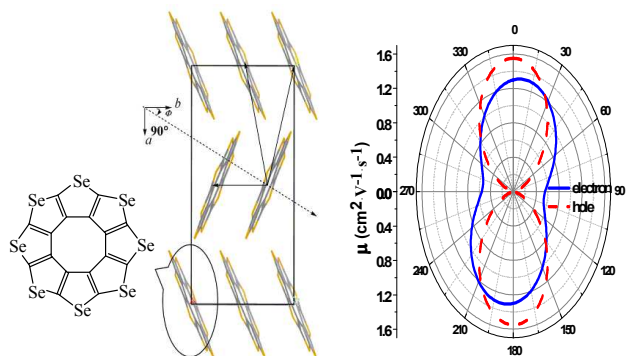
^aThe distance between two adjacent monomers and the unit is Å.

^bThe transfer integrals calculated at PW91PW91/6-31G(d,p) level and the unit is meV.

Table 5 The calculated hole and electron mobilities of $C_{16}S_4Se_4$ and $C_{16}Se_8$ ^a

Compound	Mobility ($cm^2 \cdot V^{-1} \cdot s^{-1}$)	
	Hole	Electron
$C_{16}S_4Se_4$	0.49	0.74
$C_{16}Se_8$	1.03	1.26

^a Experimental mobility of $C_{16}S_4Se_4$ is $1 \times 10^{-3} cm^2 \cdot V^{-1} \cdot s^{-1}$ [15]. Theoretical value is an upper limit of the mobility.

Table of contents entry

Crystal structure of “selfflower” $C_{16}Se_8$ was predicted on the basis of $C_{16}S_4Se_4$ crystal, and charge transport properties were investigated